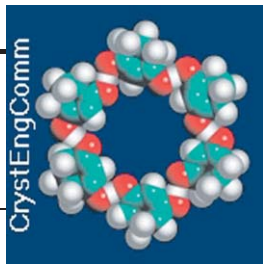

Open-framework iron phosphates: Syntheses, structures, sorption studies and oxidation catalysis†

Paper

Khalid Abu-Shandi,[a] Heiner Winkler,[b] Biao Wu[a] and Christoph Janiak*[a]

[a]*Institut für Anorganische und Analytische Chemie, Universität Freiburg, Albertstr. 21, D-79104 Freiburg, Germany. E-mail: janiak@uni-freiburg.de; Fax: 49 761 2036147 Tel: 49 761 2036127*

[b]*Institut für Physik, Universität zu Lübeck, Ratzeburger Allee 160, D-23538 Lübeck, Germany*

Received 28th March 2003, Accepted 14th May 2003
First published as an Advance Article on the web 23rd May 2003

The iron phosphates $[C_4H_{12}N_2][Fe^{II}(H_2O)_6](HPO_4)_2$ (**1**), $^3_\infty\{[NH_4][Fe^{III}_2(OH)(PO_4)_2(H_2O)]\cdot H_2O\}$ (**2**) and $^3_\infty\{[C_4H_{12}N_2][Fe^{III}_3(PO_4)_3(HPO_4)(H_2O)]\cdot \sim 0.25H_2O\}$, (**3**) were synthesized by hydrothermal methods and their single-crystal X-ray structures were determined. While compound **1** is only an extended hydrogen bonded network of its three ionic building blocks, compounds **2** and **3** are three-dimensional open-framework materials albeit of different porosity. The structure of **2** corresponds to the mineral sphenicidite. The iron building blocks in **3** are pairs of distorted edge-sharing $\{FeO_6\}$ octahedra and a five-coordinated iron atom, $\{FeO_5\}$, with a mostly trigonal-bipyramidal polyhedron. The oxidation-state assignment of **2** was backed by ^{57}Fe Mössbauer spectroscopy. Thermogravimetric analysis (TGA) of **2** and **3** shows clearly separated steps of weight loss due to the loss of water of crystallization, aqua ligand and amine template molecules. X-ray powder diffractometry proved that the empty host-frameworks were still intact after heating to 215 °C. The porous empty frameworks of **2** and **3** could be employed as sorbents towards alkanes, alcohols, chlorinated halocarbons, amines and ethers. The larger-porous framework of **3** (but not that of **2**) was found to be a catalyst for the highly regioselective oxidation of *n*-pentane to 3-pentanol with air at 15 bar and 100 °C.

Introduction

Recent years have seen numerous studies on the construction of (hydrogen)phosphato-metal network compounds.[1–14] Metal phosphates with open-framework structures, most notably aluminum phosphates (AlPO's) are of interest because of their potential applications as catalysts, molecular sieves or ion-exchange materials[2,15,16] similar to zeolites.[17] Many such compounds are prepared using organic amines as structure-directing agents by hydrothermal methods.[4–13,18–27] Redox active metal atoms are of particular interest in the construction of open-framework metal compounds for catalytic applications, *e.g.*, in oxidation catalysis.[15,16] We describe here the hydrothermal synthesis of three different iron phosphates with various degrees of porosity and the use of the more porous examples as sorption materials (active towards *n*-pentane, *n*-hexane, *n*-heptane, ethanol, *n*-propanol, *n*-butanol, CH_2Cl_2, $CHCl_3$, CCl_4, pyrrol, THF, dioxane, diethyl ether; inactive towards toluene, benzene and dioxane) and as a catalyst for the regioselective oxidation of pentane to 3-pentanol.

Results and discussion

The organic amine compounds *N*-methylpiperazine, 1,3-diaminopropane, 1,4-diaminobutane and piperazine, were tried here for application as structure directing agents in the hydrothermal synthesis of porous iron-phosphates. Utilization of the N–C-bond containing compounds *N*-methylpiperazine, 1,3-diaminopropane and 1,4-diaminobutane failed to incorporate these into an iron-phosphate framework. Instead, the N–C-bond was cleaved by a nucleophilic attack of H_2O on the N–C carbon atom to yield the corresponding alcohol and the protonated amine moiety.[28] That is, methanol and the piperazinedium dication are formed from *N*-methylpiperazine; 1,3-propanediol and 1,4-butanediol and two ammonium cations are formed from 1,3-diaminopropane and 1,4-diaminobutane, respectively, under hydrothermal conditions. Thus, hydrothermal treatment of *N*-methylpiperazinedium hydrogenphosphate dihydrate with iron(II) chloride in the presence of triethylamine in water at 180 °C yielded pink–violet crystals of composition $[C_4H_{12}N_2][Fe(H_2O)_6](HPO_4)_2$ (**1**) with di-protonated piperazine (piperazinedium, $C_4H_{12}N_2$) as a building block (eqn. (1)).

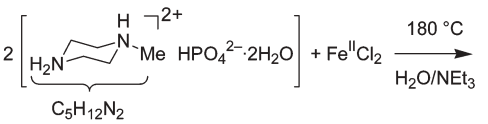

(1)

$[C_4H_{12}N_2][Fe^{II}(H_2O)_6](HPO_4)_2$ + $[C_4H_{12}N_2]Cl_2$ + 2 MeOH

1

Similarly, hydrothermal treatment of the diaminoalkanes with iron(III) chloride in phosphoric acid at 180 °C yielded

† This article is based (partly) on a presentation which will be made at the European Research Conference (EURESCO) on "Molecular Crystal Engineering - EuroConference on Design and Preparation of Molecular Materials" (Acquafredda di Maratea, Italy, 31 May - 5 June 2003) organised by the European Science Foundation and supported by the European Commission, Research DG, Human Potential Programme, High-Level Scientific Conferences, Contract HPCF-CT-2002-00270. This information is the sole responsibility of the author(s) and does not reflect the ESF or Community's opinion. The ESF and the Community are not responsible for any use that might be made of data appearing in this publication.

 DOI: 10.1039/b303498d

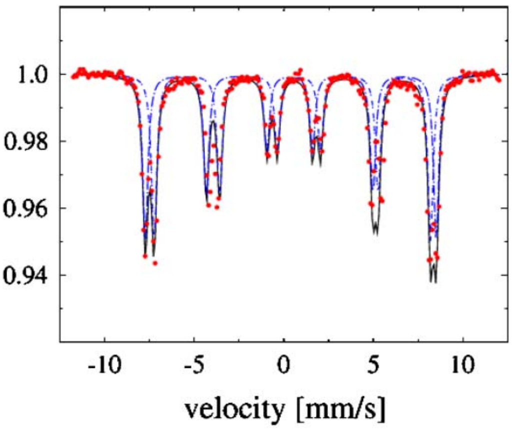

Fig. 1 Mössbauer spectra of **2** at 4.2 K. A sum of Lorentzians (solid line, parameters in text) is used to fit the experimental data (dots).

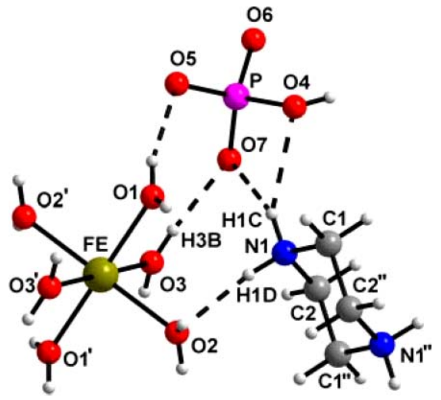

Fig. 2 Asymmetric unit of compound **1** illustrating also some of the hydrogen bonding, symmetry code: ′ = −x, −y, −z; ″ = −x, 1 − y, −z. Selected bond lengths and angles are given in Table 2 and 3. Click here to access a 3D representation.

green crystals of composition $^{3}_{\infty}\{[NH_4][Fe^{III}{}_2(OH)(PO_4)_2(H_2O)]\cdot H_2O\}$, (**2**) with the ammonium cation as a template [eqn. (2)]. Only the use of piperazine in the hydrothermal reaction with iron(II) chloride in phosphoric acid led to the direct incorporation of the piperazinedium dication in the light yellow crystals of $^{3}_{\infty}\{[C_4H_{12}N_2][Fe^{III}{}_3(PO_4)_3(HPO_4)(H_2O)]\cdot\sim 0.25H_2O\}$, (**3**) (eq. 3).

$$H_2N(CH_2)_nNH_2 + 2\ Fe^{III}Cl_3 + 2\ H_3PO_4 + 5\ H_2O \xrightarrow[H_2O]{180\ ^\circ C} \qquad (2)$$

$$^{3}_{\infty}\{[NH_4][Fe^{III}{}_2(OH)(PO_4)_2(H_2O)]\cdot H_2O\}] + NH_4Cl + 5\ HCl + HO(CH_2)_nOH$$

2

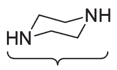

$C_4H_{10}N_2$

$$+ 3\ Fe^{II}Cl_2 + 4\ H_3PO_4 \xrightarrow[H_2O]{180\ ^\circ C} \qquad (3)$$

$$^{3}_{\infty}\{[C_4H_{12}N_2][Fe^{III}{}_3(PO_4)_3(HPO_4)(H_2O)]\cdot\sim 0.25H_2O\} + 6\ HCl + 1.5\ H_2$$

3

We note that the solid state can easily stabilize the coexistence of $[C_4H_{12}N_2]^{2+}$ and $HPO_4{}^{2-}$ or $PO_4{}^{3-}$ in an acid–base ratio different from the solution content.[29] The iron oxidation state of +3 in **2** was proven by ^{57}Fe Mössbauer spectroscopy which can help to determine whether iron atoms are Fe(II), Fe(III)[30] or mixed-valence.[31–34] The observed isomer shift and quadrupole splitting, as well as the hyperfine splitting parameters and the magnetic ordering observed at low temperature (Fig. 1) in compound **2** (Table 1), are consistent with Fe(III) (S = 5/2, high-spin) in octahedral environment.[35] Magnetic ordering has also been reported in other iron phosphates, *e.g.* $^{2}_{\infty}\{[Fe^{III}{}_2(H_2O)_2(O_3PCH_2PO_3H)_2]\cdot 2H_2O_2\}$ (antiferromagnetic),[36] $^{1}_{\infty}\{[H_3N(CH_2)_4NH_3][Fe^{III}{}_2\{CH_3C(OH)(PO_3)(PO_3H)\}_2]\cdot 2H_2O\}$ (ferromagnetic),[37] $^{2}_{\infty}\{[H_3NCH_2CH_2NH_3]_{0.5}[Fe^{III}(OH)(PO_4)]\}$ (weak antiferromagnetic)[38] and $^{3}_{\infty}\{[H_3NCH_2CH_2NH_3]_2[Fe_4O(PO_4)_4]\cdot H_2O\}$ (trapped mixed-valence, trigonal-bipyramidal Fe, anti- or canted antiferromagnetic).[33,39] In addition to these aforementioned examples, Mössbauer data are also available for other iron phosphates with octahedrally coordinated metal centers, *e.g.* $^{1}_{\infty}\{[C_4N_2H_{12}]_{1.5}[Fe^{III}{}_2(OH)(PO_4)(HPO_4)_2(H_2PO_4)]\cdot 0.5H_2O\}$[40] and $^{3}_{\infty}\{[(C_4N_3H_{16})(C_4N_3H_{15})][Fe^{III}{}_5F_4(H_2PO_4)(HPO_4)_3(PO_4)_3]\cdot H_2O\}$ (spin crossover),[41] $^{3}_{\infty}\{[C_4N_2H_{12}][Fe_4(OH)_2(HPO_4)_5]\}$ (mixed-valence) and $^{2}_{\infty}\{[C_4H_{11}N_2]_{0.5}[Fe_3(HPO_4)_2(PO_4)(H_2O)]$ (mixed-valence, also trigonal-bipyramidal Fe).[42] The two different iron atoms in **2** (see below) become apparent in the low-temperature splitting into two magnetic sextets (Fig. 1). These Mössbauer features agree with the reported magnetic frustration and three-dimensional magnetic ordering below 10 K.[43]

Compound **1** failed to produce an (open) iron-phosphate framework. Instead, the solid-state assembly in **1** is an extended hydrogen bonded network of the three ionic building blocks, the hexaaquairon(II) and the piperazinedium dications and the (two) hydrogenphosphate dianions (Fig. 2, Table 2). All protic hydrogen atoms are occupied in hydrogen bonding (Table 3). Compound **1** is isomorphous to its cobalt and nickel analog which were obtained by slow solvent evaporation at room temperature.[29]

Compound **2** forms a three-dimensional open-framework structure. The structure consists of centrosymmetric tetrameric building blocks of edge- and corner-sharing $\{FeO_6\}$ octahedra linked by $\{PO_4\}$ tetrahedra (Fig. 3) and was found to be identical with the known structure of the mineral sphenicidite.[44]

The three-dimensional connectivity of the iron-phosphate building blocks in **2** creates an open-framework structure with the ammonium cation and a water molecule of crystallization residing in channels. The channels extend primarily along the crystallographic *b*- and *c*-axes (Fig. 4). Channels along the *b*-axis contain the $NH_4{}^+$ cations, channels along the *c*-axis—the water molecules of crystallization. At the junction of the channels both "guest" molecules can be seen (Fig. 5).

Table 1 Mössbauer parameters for compound **2** [a]

Temp./K	Subspectrum	$\delta^{\alpha-Fe\,b}$/ mm s^{-1}	$\Delta E_Q{}^c$/ mm s^{-1}	$B_{hf}{}^d$/T	rel. area/%
293 (RT)	1 narrow doublet	0.40	0.51	—	100
77	1 narrow doublet	0.52	0.69	—	100
4.2	1 magnetic sextet	0.35	+0.61	49.8	50
	2 magnetic sextet	0.66	−0.36	47.3	50

[a] The errors of the hyperfine parameters are *ca.* 2% and of the relative areas 5%. [b] Isomer shift. [c] Quadrupole splitting. [d] Magnetic hyperfine field.

Table 2 Selected bonds lengths (Å) and angles (°) in compound **1**[a]

Fe-O1	2.084(2)	P-O4	1.521(2)
Fe-O2	2.110(2)	P-O7	1.525(2)
Fe-O3	2.093(2)	P-O5	1.537(2)
		P-O6	1.604(2)
O1-Fe-O2	85.77(8)	O1-Fe-O2′	94.23(8)
O1-Fe-O3	88.36(8)	O1-Fe-O3′	91.64(8)
O2-Fe-O3	89.57(9)	O2-Fe-O3′	90.43(9)

[a] Symmetry transformation: ′ = −x, −y, −z.

Table 3 Hydrogen bonding interactions (Å, °) in **1** [a]

D–H···A	D–H	H···A	D···A	D–H···A
O1–H11···O4#3	0.86(4)	1.85(4)	2.709(3)	174(3)
O1–H12···O5	0.83(3)	1.94(3)	2.757(3)	166(3)
O2–H21···O7#3	0.97(4)	1.73(4)	2.692(3)	171(3)
O2–H22···O4#4	0.85(4)	1.81(4)	2.653(3)	173(3)
O3–H31···O7	0.86(4)	1.84(4)	2.697(3)	174(3)
O3–H32···O5#1	0.83(4)	1.92(4)	2.741(3)	174(4)
O6–H6···O5#2	0.93(4)	1.69(4)	2.616(3)	175(4)
N–H1···O2	1.05(4)	1.88(4)	2.917(3)	172(3)
N–H2···O6	1.08(3)	2.09(4)	3.040(4)	146(3)
N–H2···O7	1.08(3)	2.11(3)	3.018(3)	141(3)

[a] D = Donor, A = acceptor. Symmetry transformation #1 = 1+x, y, z; #2 = −1−x, y+1/2, −z−1/2; #3 = x, −y+1/2, z+1/2; #4 = 1+x, −y+1/2, z+1/2.

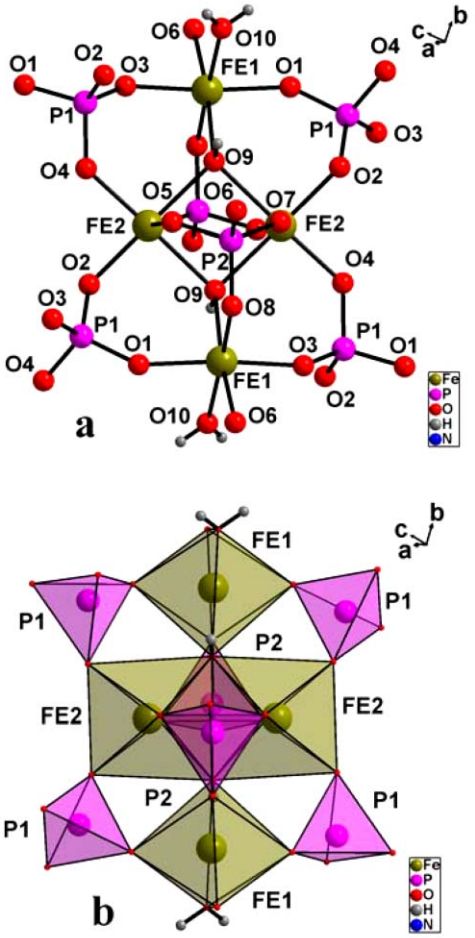

Fig. 3 Tetrameric building block in **2**. (a) Ball and stick drawing; (b) polyhedral presentation with the central atoms shown in the center of the tetrahedra. Symmetry assignments have been omitted in the atom labelling on the ball-and-stick drawing for clarity.

The water of crystallization serves as a hydrogen acceptor for the hydroyl group (O9) and the aqua ligand (010). Both guests are hydrogen bonded with all their H atoms to oxygen atoms of the phosphate groups. All protic hydrogens are involved in hydrogen bonding. Distances and angles of the hydrogen bonding interactions are given in Table 4.

The potential molecule-accessible area in the guest-depleted structure of **2** is 147 Å^3 or 16% of the unit-cell volume.[45] This has to be compared to an expected volume for H_2O of 40 Å^3 or a small molecule such as toluene of 100–300 Å^3. Thermogravimetric analyses of an air-dried sample of $^3_\infty$\{[NH_4][Fe_2(OH)-(PO_4)$_2$(H_2O)]·H_2O\}, **2** shows four cleanly separated steps of

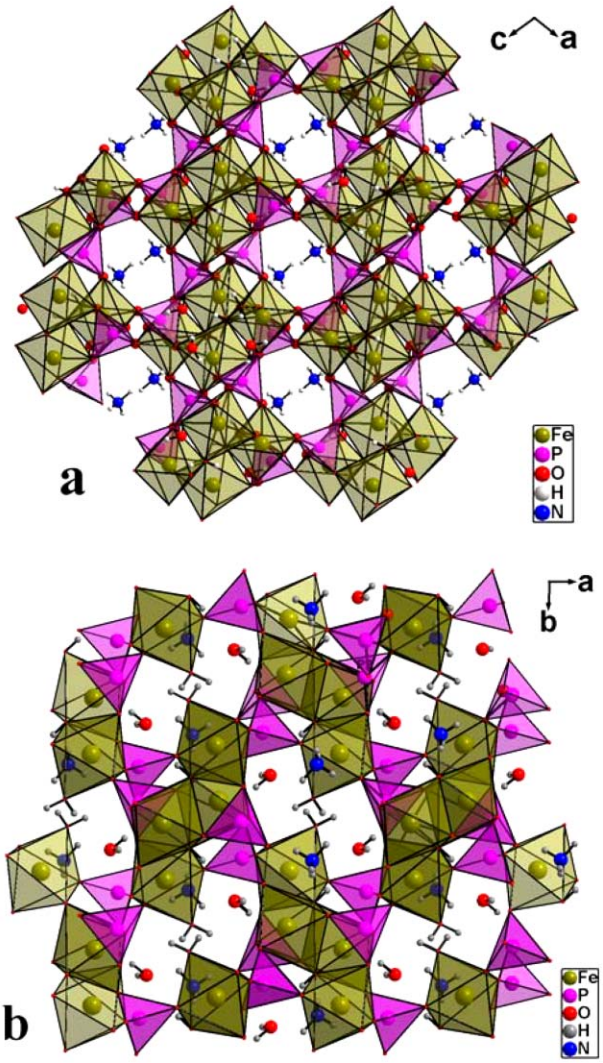

Fig. 4 Packing of the tetrameric building blocks in **2** to give a porous channel structure. (a) View along the *b*-axis showing the ammonium cation inside the channels; (b) view along the *c*-axis showing the water molecule of crystallization inside the channels. Click here to access a 3D representation.

weight loss (Fig. 6). The first three steps around 60, 130 and 205 °C, respectively, with weight losses of 4 to 5% each, can be assigned to the loss of water of crystallization (4.8% theoretical value), the aqua ligand (4.8%) and ammonia (4.6%) (not

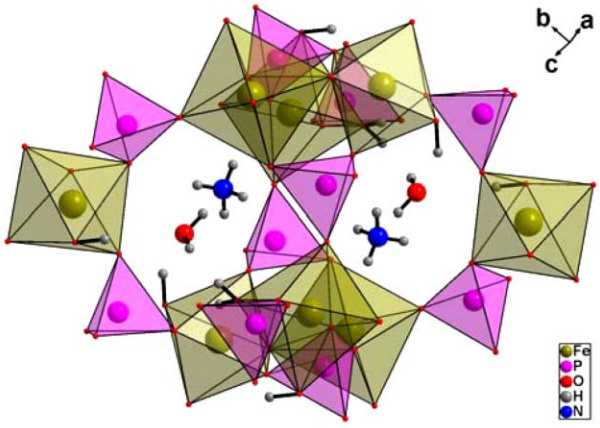

Fig. 5 Section of the open-framework structure of **2** with the ammonium cation and water molecule of crystallization both seen at a junction of the channels along the *b*- and *c*-axes (*cf.* Fig. 4).

Table 4 Hydrogen bonding interactions (Å, °) in **2**[a]

D–H···A	D–H	H···A	D···A	D–H···A
O9–H9···O11#3	0.72(5)	2.29(5)	2.997(4)	171(5)
O10–H10A···O4#4	0.71(6)	2.10(6)	2.792(4)	162(6)
O10–H10B···O11	0.74(6)	2.03(6)	2.750(4)	167(6)
O11–H11A···O4#1	0.94(6)	2.06(6)	2.935(4)	155(4)
O11–H11B···O8#2	0.72(6)	2.21(6)	2.917(4)	168(6)
N1–H1A···O7	0.70(6)	2.17(6)	2.851(5)	164(6)
N1–H1B···O5#5	0.74(6)	2.25(6)	2.956(5)	159(5)
N1–-H1C···O8#6	0.84(6)	2.29(6)	2.977(5)	140(5)
N1–H1D···O3#7	0.89(6)	2.04(6)	2.885(5)	160(5)

[a] O9 = hydroxyl group, O10 = aqua ligand, O11 = water of crystallization; D = Donor, A = acceptor. Symmetry transformation #1 = x−1/2, −y−1/2, z−1/2; #2 = −x−3/2, y−1/2, −z+1/2; #3 = −x−1, −y−1, −z; #4 = −x−1/2, y−1/2, −z+1/2; #5 = x+1/2, −y+1/2, z+1/2; #6 = −x−3/2, y+1/2, −z+1/2; #7 = −x−1, −y, −z+1.

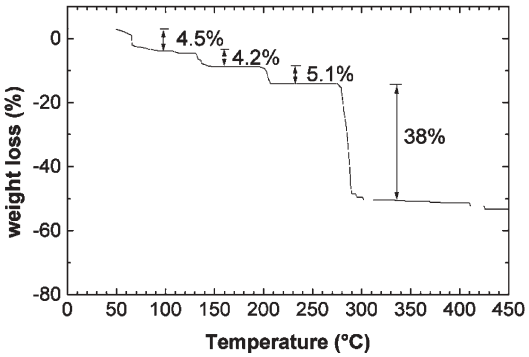

Fig. 6 TGA curve for **2**.

necessarily in this order). The weight loss of 38% between 270 and 290 °C corresponds to the evolution of P_2O_5 (calculated 38%). The remaining weight-percentage agrees with the formula of $Fe_2O_2(OH)_2$ (calculated 48%; the second OH is derived from the necessary deprotonation of NH_4^+ before leaving as NH_3). Sphenicidite has been reported to exhibit reversible dehydration and good adsorption behavior.[46]

X-ray powder diffraction was performed to test whether the open-framework of **2** was maintained on heating and guest removal. After heating to 110 °C for 5 h under vacuum and even after heating to 215 °C the diffraction data remained unchanged and both matched the simulated diffractogram from the single-crystal analysis (Fig. 7). This excellent agreement between the diffractograms shows that the open framework is retained on guest removal.

Compound **3** also forms a three-dimensional open-framework structure. The iron building blocks are pairs of distorted edge-sharing {FeO_6} octahedra and a five-coordinated iron atom, {FeO_5}, with a mostly trigonal-bipyramidal polyhedron (τ = 0.78) (Fig. 8, Table 5).[48] Atom Fe1 is coordinated by six oxygen atoms from five phosphato groups. One of the phosphato groups is chelating to Fe1 with one of the donor atoms (O3) creating a direct Fe1–O–Fe2 bridge. It is this bridge which constitutes the shared corner between the two octahedral moieties of Fe1 and Fe2. Atom Fe2 is in a disordered ligand environment and on an average basis coordinated by one aqua ligand and five oxygen donors from four phosphato groups (one of them, P3, chelating). However, from the coordinating atoms which can be simultaneously present, it is more likely that individual Fe2 atoms are coordinated either by two aqua ligands and four oxygen donors from four phosphato groups (all monodentate) or by six oxygen atoms from five phosphato groups (P3 chelating). The trigonal-bipyramidal atom Fe3 has five oxygen donors from five phosphato groups. One of the

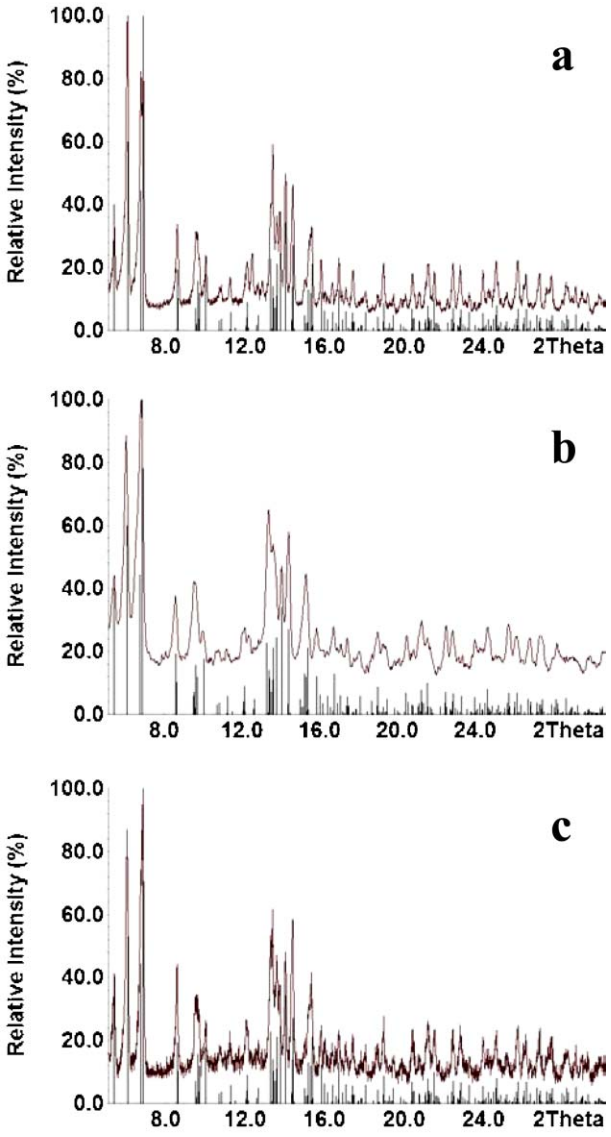

Fig. 7 X-ray powder diffractograms of **2**: (a) as synthesized; (b) after heating to 110 °C for 5 h under vacuum; and (c) after heating to 215 °C for 2 h under vacuum. The vertical bars represent the simulated diffractogram from the single-crystal data.[47]

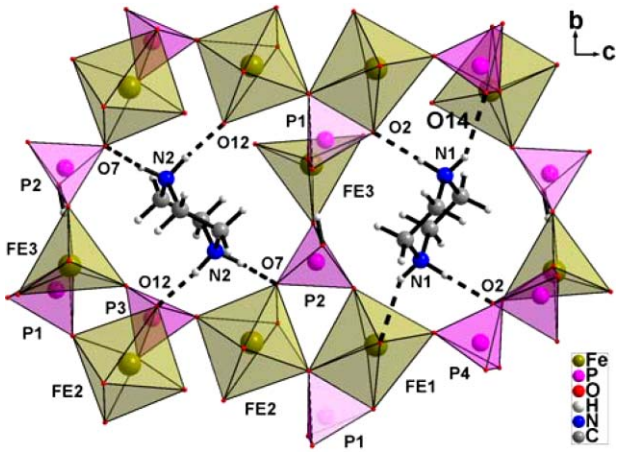

Fig. 8 Section of the open-framework structure of **3** showing the phosphate and octahedral or five-coordinated iron building blocks with the piperazinedium dication residing in the channels along the *a*-axis. The disordered phosphate groups around P2′ and P3′ are not shown for clarity. Selected bond lengths and angles are given in Table 5 and 6. Click here to access a 3D representation.

Table 5 Selected bonds lengths (Å) and angles (°) in compound **3**[a]

Fe1–O16#1	1.891(3)	Fe2–O3	2.011(3)
Fe1–O5	1.947(3)	Fe2–O12′#2	2.053(6)
Fe1–O14	1.970(3)	Fe2–O7	2.110(6)
Fe1–O15#2	1.994(3)	Fe2–O21	2.119(6)
Fe1–O2	2.029(3)	Fe2–O12	2.151(6)
Fe1–O3	2.279(3)	Fe3–O13	1.873(3)
Fe2–O7′	1.814(6)	Fe3–O6#4	1.893(3)
Fe2–O10#3	1.950(3)	Fe3–O11	1.897(3)
Fe2–O9	2.010(3)	Fe3–O4	1.975(3)
Fe2–O21′	2.020(6)	Fe3–O1#5	1.979(3)

Only angles given which deviate more than ±5° from 90° or ±10° from 180°, respectively.

O2–Fe1–O3	67.1(1)[b]	O9–Fe2–O7	80.2(2)
O5–Fe1–O2	156.8(1)	O9–Fe2–O12	63.7(2)[b]
O14–Fe1–O15#2	174.3(1)	O9–Fe2–O12′#2	157.6(2)
O16#1–Fe1–O5	99.0(1)	O9–Fe2–O21	160.6(2)
O16#1–Fe1–O2	103.9(1)	O9–Fe2–O21′	106.2(2)
O3–Fe2–O12′#2	95.6(2)	O10#3Fe2–O12′#2	80.3(2)
O3–Fe2–O21	80.9(2)	O10#3–Fe2–O21	96.3(2)
O7′–Fe2–O9	101.4(3)	O12′#2–Fe2–O7	120.6(3)
O7′–Fe2–O12	165.0(3)	O12′#2–Fe2–O12	95.1(1)
O7′–Fe2–O12′#2	99.4(3)	O4–Fe3–O1#5	177.3(1)
O7–Fe2–O12	143.9(2)	O11–Fe3–O6#4	111.5(2)
O7–Fe2–O21	82.6(3)	O13–Fe3–O6#4	117.7(2)
O7′–Fe2–O21′	152.2(3)	O13–Fe3–O11	130.8(2)

[a] Symmetry transformations: #1 = $-x-1$, $-y$, $-z+1$; #2 = $x+1$, y, z; #3 = $-x-1$, $-y$, $-z$; #4 = $x-1$, $y-1$, z; #5 = $x-1$, y, z. Primed atoms indicate disorder to the unprimed atom of the same number. Around Fe2 only angles for simultaneously possible ligand atoms are given according to the disorder model discussed in the text. [b] Chelating PO_4-groups.

phosphate groups (P2, P2′) bridges only between three iron atoms, while the other three PO_4 groups bridge four iron atoms each. Thus, P2 was taken as a hydrogenphosphato group to reach electroneutrality. Bond valence sum calculations done on the structure of **3** assign an oxidation state of +3 to all three crystallographically different iron atoms (calc. Fe1 3.1, Fe2 2.9 or 3.3 depending on the disorder model, Fe3 3.2).[49,50] The piperazinedium template molecule resides in channels along the *a*-axis. Unlike the iron-phosphate framework the template molecule could be readily located and did not exhibit any disorder. The piperazinedium dication is firmly anchored through hydrogen bonding to the phosphate oxygen atoms (Fig. 8, Table 6). The primary structural features of **3** are very similar to those of a yellow compound of formula $(C_4H_{12}N_2)[Fe_6(PO_4)_6(HPO_4)_2(H_2O)_2]\cdot H_2O$ reported by Zima and Lii.[51] The latter compound was obtained starting from $FeCl_3$ instead of $FeCl_2$ as by us. Furthermore, there are some variations in the cell constants which may be due to a different water content.

The potential molecule-accessible area in the template-depleted structure of **3** is 222 Å^3 or 26% of the unit-cell volume.[45] This rises to 240 Å^3 or 28% if also the aqua ligand

Table 6 Hydrogen bonding interactions (Å, °) in **3**[a]

D–H···A	D–H	H···A	D···A	D–H···A
O8–H8A···O1#1[b]	0.91	1.90	2.814(4)	178.2
O8–H8B···O31#4[b]	0.82	1.66	2.386(4)	147.3
N1–H1A···O2#2	0.91	1.83	2.737(4)	174.1
N1–H1B···O14	0.91	2.15	2.979(4)	150.5
N2–H2A···O7#3	0.91	1.99	2.805(4)	147.5
N2–H2B···O12	0.91	1.64	2.531(4)	164.5
N2–H2B···O21′	0.91	2.19	3.014(4)	150.4

[a] D = Donor, A = acceptor. Symmetry transformation #1 = x, $y+1$, z; #2 = $-x-1$, $-y$, $-z+1$; #3 = $-x-1$, $-y$, $-z$; #4 = $x-1$, y, z. [b] Two hydrogen positions possible on O8 (of HPO_4) for hydrogen bonding.

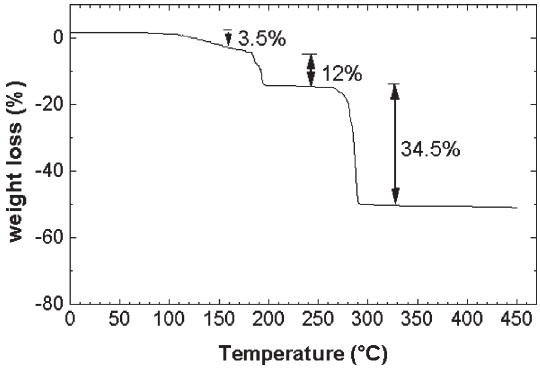

Fig. 9 TGA curve for **3**.

and water of crystallization are removed. Thermogravimetric analysis of an air-dried sample of $^3_\infty\{[C_4H_{12}N_2][Fe_3(PO_4)_3(HPO_4)(H_2O)]\cdot\sim 0.25H_2O\}$, **3**, shows three steps of weight loss (Fig. 9). The first two steps, which are not cleanly separated amount to a weight loss of *ca.* 16% between 100 and 200 °C. This weight loss can be assigned to the loss of water (3.4% theoretical value) and piperazine, $C_4H_{10}N_2$ (13.0%). The weight loss of 34% between 270 and 290 °C corresponds to the partial evolution of 1.5 (out of 2) equivalents of P_2O_5 (calculated 32%). The remaining weight-percentage agrees with a formula of $Fe_3O_{2.5}(OH)_2(HPO_4)$ (calculated 51%, the two OH are derived from the necessary deprotonation of piperazinedium before leaving as $C_4H_{10}N_2$).

X-ray powder diffraction showed that the open-framework of **3** was maintained on heating to 110 °C for 5 h under vacuum and even after heating to 215 °C with the guest removal. After heating the diffraction data remained unchanged and both matched the simulated diffractogram from the single-crystal analysis (Fig. 10).

The three title compounds display quite different colors: **1** pink-violet, **2** green, **3** light-yellow. We note that the color of iron(II) and iron(III) complexes in a ligand field of (nitrogen and) oxygen donors can vary to a large extent from (dark-)red[52] over brown[53] to (red-)orange(-yellow)[54] and light-/yellow-green[55] for Fe(II) and from (dark-)blue,[56] (dark-)red[57] to orange/yellow[58] and (dark-)green[59] for Fe(III). More intense colors usually arise from charge-transfer absorptions (perhaps as in **1**). The color is not only affected by the ligand and its ligand-field but also by the spin state (low-/high-spin configuration) of the iron atom or the possibility of electronic coupling (as in **2**) between adjacent iron centers. A not very intense (yellow) color, as in **3**, is expected for high-spin-d^5 Fe(III) with only spin-forbidden d–d transitions and CT absorption commening in the far visible/near UV (blue-violet region).

Sorption studies

Table 7 summarizes the results of sorption studies using samples of **2** or **3** which were heated in vacuum at 110 °C for 5 h and thereafter are termed **2*** or **3***, respectively. It is evident that **2*** and **3*** exhibit a certain size and function selectivity in the absorption process. The smaller cavities in **2*** do not absorb THF, the non-functional *n*-alkanes and pyrrol when compared to **3***. If absorption takes place with both sorbents, then they absorb the same guest amount within experimental error. When a mixture of absorbable guests is offered for absorption then only the smaller guest is selectively absorbed, except for the chloromethanes, where $CHCl_3$ only is absorbed out of a $CH_2Cl_2/CHCl_3/CCl_4$ mixture. The competition *n*-butanol/diethyl ether shows a clear preference for the absorption of polar alcohols over much less polar guests of similar size. The sorption properties for the non-porous compound $^3_\infty[Fe^{II}{}_5Fe^{III}{}_2(PO_4)_2(H_{0.5}PO_4)_4]$[60] were negatively tested

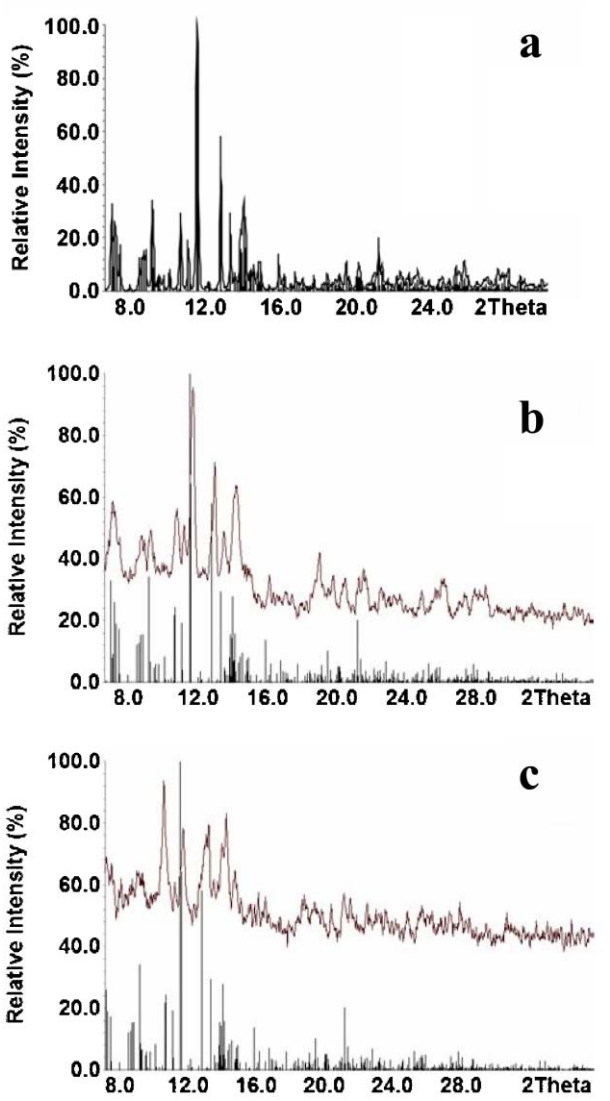

Fig. 10 X-ray powder diffractograms of **3** (a) as synthesized, (b) after heating to 110 °C for 5 h under vacuum, and (c) after heating to 215 °C for 2 h under vacuum. The vertical bars represent the simulated diffractogram from the single-crystal data.[47]

towards pentane and ethanol to exclude the possibility of an outer-surface sorption.

The gas chromatographic measurements were followed by X-ray powder diffraction (XRPD) data collections. XRPD experiments indicate that the sorbents **2*** and **3*** are capable of accommodating solvents within the cavities of the structure without disturbing the framework. The powder patterns of **2*** and **3*** after the sorption of different guest molecules exhibit some extra diffraction peaks at *ca.* $2\theta = 10.5°$ for **2*** and $2\theta = 18.5°$ and 21.3° for **3*** (Fig. 11). These peaks are most likely due to the absorbed organic guest species and are in agreement with peaks reported for other host–guest systems.[61] The peaks originating from the host lattice should be invariant if the host framework remains intact, that is unaffected by the guest exchange. The XRPD measurements for **2*** and **3*** before and after guest adsorption were carried out in the same way.

Catalytic studies

The catalytic oxidation of *n*-pentane by molecular oxygen was studied using samples of **2** or **3** which were heated in vacuum at 215 °C for 2 h and thereafter are termed **2**** or **3****, respectively. X-ray powder diffraction had already shown that the framework remained intact (*cf.* Fig. 7 and 10). Linear alkanes, such as *n*-pentane, resist attack by boiling nitric acid,

Table 7 Selected sorption results with **2*** and **3***[a]

Guest[c]\sorbent	**2***[b]	**3***[b]
Toluene	n	n
Benzene	n	n
THF	n	a (83)
Ethanol	a (88)	a (93)
n-Propanol	a (97)	a (92)
n-Butanol	a (95)	a (85)
Ethanol/*n*-propanol	a/n (95/0)	a/n (95/0)
Propanol/*n*-butanol	a/n (95/0)	a/n (92/0)
Diethyl ether	a (99)	a (99)
n-Butanol/diethyl ether	a/n (87/0)	a/n (95/0)
n-Pentane	n	a (87)
n-Hexane	n	a (87)
n-Heptane	n	n
n-Pentane/*n*-hexane	n/n	a/n (83/0)
n-Hexane/*n*-heptane	n/n	a/n (97/0)
CH_2Cl_2	a (64)	a (89)
$CHCl_3$	a (96)	a (81)
CCl_4	a (96)	a (88)
$CH_2Cl_2/CHCl_3/CCl_4$	n/a/n (0/86/0)	n/a/n (0/91/0)
Dioxane	n	n
Pyrrol	n	a (78)
THF/pyrrol	n/n	n/a (0/94)

[a] Selected quantitative data for sorption experiments carried out with 15 mg of **2*** or **3*** and 10 μL of a binary 1/1-molar guest/toluene[c] mixture, 15 μL of a ternary 1/1/1-molar guest1/guest2/toluene mixture and 20 μL of a 1/1/1/1-molar guest1/2/3/toluene mixture. Numbers in parentheses are percentages in the reduction of the absorbed guest peak area intensity (from GC). The reduction refers relative to the sorbent-free vial (blank) as the standard for the starting composition, self-corrected for changes (reductions) of the more volatile component; the internal toluene standard allowed for the comparison of both values; GC/MS reproducibility of the quantitative data was within 10%; a = absorbed, n = not absorbed. [b] Obtained from **2** or **3** after heating at 110 °C for 5 h under vacuum. [c] Toluene added as an internal standard for each prospective guest.

concentrated sulfuric acid, chromic acid, or potassium permanganate. But even if suitable catalysts were found to facilitate modest reaction with these (normally) aggressive reagents, these oxidants are not any more environmentally acceptable. Hydrogen peroxide and oxygen (air) are far superior oxidants to employ if suitable catalysts can be developed for their use.[62,63]

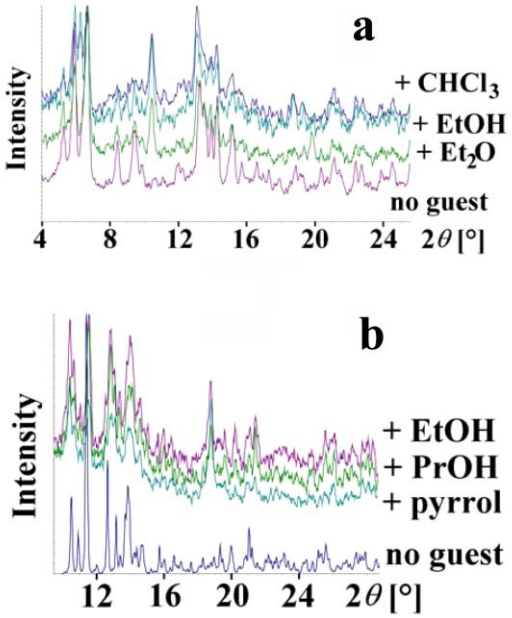

Fig. 11 Examples of X-ray powder patterns for the frameworks **2*** (a) and **3*** (b) before and after reaction with different guest molecules.

When a mixture of *n*-pentane and toluene (internal standard) was subjected to an oxidative catalytic test with **2**** and **3**** there was, unsurprisingly, no conversion of the toluene molecule, as it is too large to access the active metal sites within these frameworks (*cf.* sorption studies). On the other hand, a conversion of *n*-pentane has been found for **3**** but neither for **2**** nor for *n*-pentane/air alone under the same conditions. Compound **2*** was shown above not to absorb *n*-pentane, presumably because of its smaller pore size together with the hydrophilic character of the pore. Thus, lack of absorption fails to initiate the catalytic oxidation reaction which argues that the successful catalytic reaction with **3**** does indeed take place within the pores and that it is not a surface reaction.

The catalysis experiments were monitored by GC/MS in selected time intervals up to a total reaction time of 60 h. From the change in area ratio of pentane to toluene together with the appearance of the new peak, the pentane conversion could be calculated as shown in Fig. 12. Even with **3**** the catalytic oxidation of pentane is not a very fast and efficient reaction. A pentane conversion of 25% was reached after 60 h for 15.9 mL pentane and 50 mg catalyst under 15 bar air (20 °C) at 100 °C. This may be compared, however, to the air-oxidation of cyclohexane to a mixture of cyclohexanol, cyclohexanone, adipic acid, valeraldehyde and valeric acid by FeAlPO-5 or MnAlPO-5 where at the most, 7% conversion (without the use of a free-radical initiator) could be reached after 24 h (1.5 MPa, 130 °C).[64] Also, oxidation of *n*-hexane to mainly hexanoic acid using CoAlPO-18 or CoAlPO-36 gave only less than 10% conversion after 25 h in the absence of free-radical initiators.[65] Mechanistically it is well known that the oxidation of alkanes with the help of transition metal ions generally involves the participation of free radicals.[65,66] Consequently, conversion can be increased with the metal-phosphate frameworks by adding a free-radical initiator such as *tert*-butyl hydroperoxide.[64,65,67]

Still, the catalytic oxidation of *n*-pentane by **3**** is remarkable in that it is highly regioselective. By GC/MS, 3-pentanol could be identified as the only product out of at least seven possible ones (Fig. 13). No further GC traces besides those of the pentane and toluene starting material were detected. Retention time and mass spectrometric fragmentation pattern of the reaction product were fully matched to an authentic 3-pentanol sample (from Merck). In addition, further authentic samples of 1- and 2-pentanol (from Merck) revealed different retention times and fragmentation pattern for these isomers for ruling out any ambiguity. The more stable secondary over primary alkyl-radical intermediates and, subsequently, the formation of 2- or 3-pentanol are expected for a radical-oxidation process. Still, the sole formation of 3-pentanol cannot be reasoned at this stage and will be the subject of further studies.

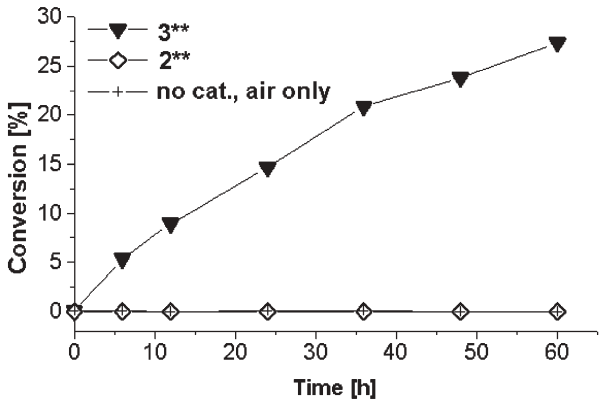

Fig. 12 Conversion of *n*-pentane using air catalyzed with **3****. The presence of **2**** or no catalyst led to no conversion.

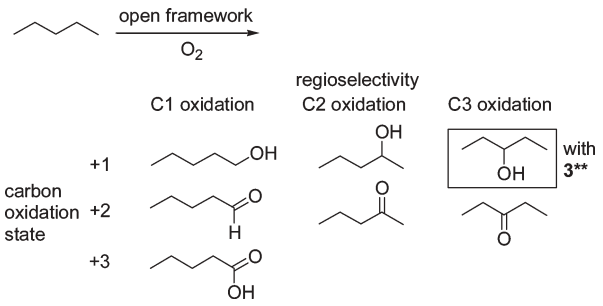

Fig. 13 Possible products for the oxidation of pentane.

Experimental part

IR spectra (KBr pellet) were measured on a Bruker Optik IFS 25. Elemental analyses were obtained on a VarioEL from Elementaranalysensysteme GmbH. Iron analyses were carried out by atomic absorption spectroscopy on a Vario 6 flame photometer from Analytik Jena. NMR spectra were recorded on a Bruker Avance DPX200 spectrometer (200.1 MHz for ^{1}H) with calibration against the solvent signal (D_2O 4.87 ppm). X-ray powder diffractometry was done on a Stoe STADI P with Debye-Scherrer geometry, Mo-Kα radiation (λ = 0.7093 Å), a Ge(111) monochromator and the samples in glass capillaries on a rotating probe head. Thermogravimetric analysis was done on a simultaneous thermoanalysis apparatus STA 409 from Netzsch under nitrogen (heating rate 5 K min^{-1}). $FeCl_2 \cdot 3H_2O$ and $FeCl_3 \cdot 6H_2O$ were obtained from Merck.

^{57}Fe Mössbauer spectroscopy

^{57}Fe Mössbauer spectra were recorded with a conventional spectrometer in constant-acceleration mode with a ^{57}Co[Rh] source. The velocity calibration was performed with an α-Fe foil at room temperature, for which the magnetic hyperfine splitting is known with high accuracy. The measured isomer shifts are referred to this α-Fe standard. The experimental spectra were fitted by a sum of Lorentzian lines by means of a least-squares procedure.

X-ray crystallography

Data collection: Bruker AXS with CCD area-detector, Mo-Kα radiation (λ = 0.71073 Å), graphite monochromator, double-pass method ϕ–ω-scan, data collection and cell refinement with SMART,[68] data reduction with SAINT,[68] experimental absorption correction with SADABS.[69]

Structure Analysis and Refinement: The structure was solved by direct methods (SHELXS-97);[70] refinement was done by full-matrix least squares on F^2 using the SHELXL-97 program suite.[70] All non-hydrogen positions were found and refined with anisotropic temperature factors. In **1** the hydrogen atoms on oxygen of the water molecule and the hydrogenphosphato group were found and refined with isotropic temperature factors. The hydrogen atoms on nitrogen of the piperazinedium cation were found and refined with U_{eq}(H) = 1.5 U_{eq}(N). Hydrogen atoms on carbon of piperazinedium were calculated with appropriate riding models (AFIX 23) and U_{eq}(H) = 1.2 U_{eq}(C). In **2** the hydrogen atoms on the hydroxy group (O9), aqua ligand (O10), the water molecule of crystallization (O11) and the ammonium moiety (N1) were found from the difference Fourier map and their position could be freely refined with U_{eq}(H) = 1.5U_{eq}(O,N). Crystal data were as given before.[44] In **3** the hydrogen atoms on piperazinedium were calculated with appropriate riding models (AFIX 23) and U_{eq}(H) = 1.2 U_{eq}(C,N). The hydrogen atom on HPO_4 was placed in a position calculated for an appropriate hydrogen bond to O1 with U_{eq}(H) = 1.5 U_{eq}(O). One HPO_4 ligand was

Table 8 Crystal data for compounds **1** and **3**

	1	**3**
Formula	$C_4H_{26}FeN_2O_{14}P_2$	$C_4H_{13}Fe_3N_2O_{17.25}P_4$
M	444.06	656.59
Crystal size/mm	0.24 × 0.11 × 0.11	0.18 × 0.08 × 0.07
Crystal description	Isometric	Isometric
T/K	213(2)	213(2)
θ range/°	2.64–28.63	1.33–28.77
h; *k*; *l* range	−8,8;−11,12; −16,16	−8,8;−11,12; −20,20
Crystal system	Monoclinic	Triclinic
Space group	*P*2(1)/*c*	*P*-1
a/Å	6.317(4)	6.355(2)
b/Å	9.643(5)	9.166(2)
c/Å	12.877(7)	15.311(4)
α/°	90	90.270(4)
β/°	92.574(9)	91.338(4)
γ/°	90	106.594(4)
V/Å^3	783.6(8)	854.4(4)
Z	2	2
D/g cm^{-3}	1.882	2.552
F(000)	464	654
μ/mm^{-1}	1.242	2.988
Absorption correction	SADABS	SADABS
Max/min transmission	0.8755/0.7548	0.8181/0.6153
Measured reflections	4479	7722
Unique reflections (R_{int})	1808 (0.0277)	4000 (0.0289)
Obs. reflections [$I > 2\sigma(I)$]	1370	2917
Parameters refined	140	330
Max/min $\Delta\rho$/e Å^{-3} [a]	0.593/−0.639	1.307/−1.081
*R*1/*wR*2 [$I > 2\sigma(I)$][b]	0.0330/0.0819	0.0419/0.0955
*R*1/*wR*2 (all data) [b]	0.0471/0.0875	0.0617/0.1054
Goodness-of-fit on F^2 [c]	1.020	1.055
Weight. scheme *w*; *a*/*b*[d]	0.0471/0.0000	0.0522/0.0000

[a] Largest difference peak and hole. [b] $R1 = [\Sigma(||F_o| - |F_c||)/\sum|F_o|]$; $wR2 = [\Sigma[w(F_o^2 - F_c^2)^2]/\sum[w(F_o^2)^2]]^{1/2}$. [c] Goodness-of-fit = $[\Sigma[w(F_o^2 - F_c^2)^2]/(n - p)]^{1/2}$. [d] $w = 1/[\sigma^2(F_o^2) + (aP)^2 + bP]$ where $P = (\max(F_o^2 \text{ or } 0) + 2F_c^2)/3$.

assumed because of electroneutrality for all Fe in the formal +3 oxidation state. Oxygen atom O8 was chosen for the hydrogen atom since it is the only O atom with no bond to Fe. The phosphato groups of P2 and P3 were subject to disorder coupled together with the aqua ligand (O21, O21′) on Fe2. As part of the disorder around P2 a water molecule of crystallization (O31, not fully occupied) could be located. O8′ was refined with an isotropic thermal parameter. The hydrogen atoms of the water molecules were neither found nor calculated, hence there is a deviation in the chemical formula moiety composition and the chemical formula sum by 2.5 hydrogen atoms. Graphics were obtained with DIAMOND.[71] Crystal data and details on the structure refinement are given in Table 8. The structural data has been deposited with the Cambridge Crystallographic Data Center (CCDC) with reference numbers 207258–207260. See http://www.rsc.org/suppdata/ce/b3/b303498d/ for crystallographic data in CIF or other electronic format.

Sorption studies

The samples for the sorption studies were prepared by heating 100 mg of compound **2** or **3** to 110 °C for 5 h under vacuum. After cooling the obtained guest-depleted materials **2*** and **3*** were stored under argon. The sorption studies were carried out in a 2 mL vial covered with a screw cap and a Teflon septum. Chosen weights (15 mg) of **2*** and **3*** were transfered to these vials. Accurate volumes (10 to 20 μL) of the guest mixture for the sorption studies were added to the vials with a 10 μL microsyringe. An empty vial was filled with the guest mixture as a point of reference to account for changes in the mixture due to the different vapor pressures/volatilities of the solvents employed as guests. The vials were stored in the refrigerator for 2 h at 2 °C to allow for equilibration. Then the solvent mixture in both the sorbent-containing and the sorbent-free vial were quantitatively analyzed by gas chromatography. An HP 5890 Series II GC fitted with an Ultra2 column (stationary phase Ph-Me-silicone, 50 m, 0.2 mm od, 0.11 mm id, carrier gas He) and connected to a quadrupole mass spectrometer HP 5989A (EI ionization) was employed. Alternatively, a pe Erba GC6000 Vega Series (column: dimethylpolysiloxane, 25 m, 0.32 mm od, 0.25 mm id, carrier gas H_2) connected to an FID was used. Toluene was found not to be absorbed by **2*** and **3*** and therefore was included as an internal standard within each guest mixture. The area ratios of the other guest species were referenced with respect to the one of toluene.

Catalytic oxidation studies

The samples for the catalytic studies were prepared by heating 100 mg of compound **2** or **3** to 215 °C for 2 h under vacuum. After cooling the obtained guest-depleted materials **2**** and **3**** were stored under argon. The catalysis studies were carried out in a 60 mL high-pressure stainless-steel autoclave, fitted with a pressure manometer, a gas inlet and drain valve (underneath the solution surface) to collect samples without depressurizing the autoclave. The autoclave was charged with 50 mg of catalyst of **2**** or **3**** (0.156 mmol of **2**** assuming that $2H_2O + NH_3$ were removed by heating and 0.091 mmol of **3**** assuming that $1.25H_2O + C_4H_{10}N_2$ were removed by heating up to 215 °C) followed by 15.9 mL of pentane and 1.1 mL of toluene (internal standard). For the blank measurement only the solvents were added. The autoclave was pressurized with dry air to 15 bar and heated to 100 °C. During heating the pressure rose to *ca*. 17 bar. Samples were drawn after 0, 6, 12, 24, 36, 48 and 60 h from the pressurized autoclave, which was briefly cooled to room temperature. Sample aliquots were two-times 300 μL. The first 300 μL were discarded to clear the dead-volume parts of the drain-valve. Samples were analyzed by GC/MS (HP 5890 Series II/5989A, as described above).

Synthesis

***N*-methylpiperazinedium hydrogenphosphate dihydrate, $[C_5H_{14}N_2]HPO_4{\cdot}2H_2O$.** To a solution of *N*-methylpiperazine (6.66 mL, 60 mmol) in 10 mL of water was added H_3PO_4 (5 mL, 85 wt.%, $d = 1.70$ g mL^{-1}, 73.75 mmol) with vigorous stirring. The mixture was heated to 110 °C for 20 h. After cooling to room temperature a yellow oil was produced and 20 mL of absolute ethanol were added with slow stirring to produce the title compound as a colorless precipitate (yield 9.10 g, 72%). $C_5H_{19}N_2O_6P$ (234.19): calc. C 25.64, H 8.18, N 11.96; found C 25.04, H 7.68, N 11.75%. ^{1}H NMR (D_2O): 2.84 (s, CH_3), 3.31 (t, CH_2, $J = 4.77$ Hz), 3.56 (t, CH_2, $J = 4.77$ Hz). IR (major peaks only): 3377 (νOH), 1638 (νC–N), 1463 (νP=O), 1030 (νP–O).

Hexaaquairon(II)-H2piperazinedium-bis(hydrogenphosphate), $[C_4H_{12}N_2][Fe^{II}(H_2O)_6](HPO_4)_2$, (1). Under a positive pressure of argon $FeCl_2{\cdot}3H_2O$ (0.353 g, 1.50 mmol) was dispersed in 5 mL of degassed water in a Schlenk flask to give a yellowish-green, clear solution. To this solution *N*-methylpiperazinedium hydrogenphosphate dihydrate (0.60 g, 2.56 mmol) was added with continuous stirring, followed by triethylamine (TEA) (0.65 mL, 4.70 mmol). The TEA was needed to adjust the pH of the resulting solution to *ca*. 8. The mixture was stirred at room temperature for 30 min. The solution was transferred to a Teflon-lined stainless-steel autoclave and heated at 180 °C for 40 h followed by cooling at a rate of 10 °C min^{-1}. Pink–violet crystals were collected by filtration (yield 310 mg, 55% based on

phosphate). $C_4H_{26}FeN_2O_{14}P_2$ (444.06): calc. C 10.82, H 5.90, N 6.31; found C 10.44, H 5.63, N 6.75%. IR (major peaks only): 3500 (br, *v*OH), 3037 (*v*N–H), 1463 (*v*PO), 956 (*v*P–O). ^{1}H NMR (D_2O): 2.21 (s, br, CH_2).

Ammonium-[aqua(μ_3-hydroxo)bis(μ_4-phosphato)diferrate(III)]-hydrate, $^3_\infty${[NH$_4$][Fe$^{III}_2$(OH)(PO$_4$)$_2$(H$_2$O)]·H$_2$O}, (2). A mixture of $FeCl_3·6H_2O$ (0.40 g, 1.5 mmol), H_2O (10 mL), 1,3-diaminopropane (0.55 g, 0.63 mL, 7.5 mmol) or 1,4-diaminobutane (0.66 g, 0.75 mL, 7.5 mmol) and H_3PO_4 (0.50 mL, 85 wt.%, d = 1.70 g mL^{-1}, 7.5 mmol) was placed in a Teflon-lined stainless steel autoclave without stirring and heated at 180 °C for 72 h followed by cooling at a rate of 10 °C min^{-1}. Green crystals were collected by filtration (yield 210 mg, 75%). The synthesis was reproducibly repeated eight times using either 1,3-diaminopropane or 1,4-diaminobutane. Product identity was verified by X-ray powder diffractometry. $Fe_2NH_9O_{11}P_2$ (372.72): calc. C 0.00, H 2.43, N 3.76, Fe 29.97; found C 0.00, H 2.50, N 4.10, Fe 29.85%. IR (major peaks only): 3487 (br, *v*OH), 1428 (*v*PO), 983 (*v*P–O).

H2piperazinedium-aqua(μ_3-hydrogenphosphato)(tris-μ_4-phosphato)-tri-iron(III)-0.25hydrate, $^3_\infty${[C$_4$H$_{12}$N$_2$][Fe$^{III}_3$(PO$_4$)$_3$(HPO$_4$)(H$_2$O)]·~0.25H$_2$O}, (3). Under a positive pressure of argon $FeCl_2·3H_2O$ (0.353 g, 1.50 mmol) was dispersed in 7 mL of degassed water in a Schlenk flask to give a yellowish-green, clear solution. To this solution piperazine (0.64 g, 7.5 mmol) was added with continuous stirring followed by H_3PO_4 (0.86 mL, 85 wt.%, d = 1.70 g mL^{-1}, 15.0 mmol). The mixture was stirred at room temperature for 30 min. The solution was transferred to a Teflon-lined stainless-steel autoclave and heated at 180 °C for 40 h followed by cooling at a rate of 10 °C min^{-1}. Light-yellow crystals were collected by filtration (yield 175 mg, 54%). The synthesis was reproducibly repeated seven times. Product identity was verified by X-ray powder diffractometry. $C_4H_{15.5}Fe_3N_2O_{17.25}P_4$ (659.11): calc. C 7.29, H 2.37, N 4.25, Fe 25.42; found C 7.21, H 2.32, N 4.17, Fe 25.64%. IR (major peaks only): 3475 (br, *v*POH), 3128 (*v*N–H), 1459 (*v*PO), 1042 (*v*P–O).

Acknowledgements

The research was supported by the Fonds der Chemischen Industrie and the graduate college "Unpaired electrons" at the University of Freiburg through a fellowship to K.A.-S. We thank Prof. A. X. Trautwein, Universität zu Lübeck, for his support and helpful discussions.

References

1 C. N. R. Rao, S. Natarajan, A. Choudhury, S. Neeraj and A. A. Ayi, *Acc. Chem. Res.*, 2001, **34**, 80.
2 Review: A. K. Cheetham, G. Férey and T. Loiseau, *Angew. Chem., Int. Ed. Engl.*, 1999, **38**, 3268.
3 Gallophosphate polymorphs, theory: S. Girard, J. D. Gale, C. Mellot-Draznieks and G. Férey, *J. Am. Chem. Soc.*, 2002, **124**, 1040.
4 $^3_\infty${[C$_4$N$_2$H$_{12}$][Co$_{0.14}$Zn$_{1.86}$(PO$_4$)(H$_{1.5}$PO$_4$)$_2$]}: X. Chen, Y. Zhao, R. Wang, M. Li and Z. Mai, *J. Chem. Soc., Dalton Trans.*, 2002, 3092.
5 $^3_\infty${[C$_2$NH$_8$][Zn$_3$(PO$_4$)(HPO$_4$)$_2$]·H$_2$O} and $^3_\infty${[(C$_2$NH$_8$)(H$_3$O)][Zn$_4$(PO$_4$)$_3$(H$_2$O)]$_2$·H$_2$O}: S. Neeraj and A. K. Cheetham, *J. Chem. Soc., Chem. Commun.*, 2002, 1738.
6 Open-framework zinc phosphates: Y. Song, J. Yu, G. Li, Y. Li, Y. Wang and R. Xu, *J. Chem. Soc., Chem. Commun.*, 2002, 1720.
7 $^2_\infty${[NH$_4$][(V$_2$O$_3$(4,4′-bipy)$_2$(H$_2$PO$_4$)(PO$_4$)$_2$]·0.5H$_2$O}: L.-I. Hung, S.-L. Wang, H.-M. Kao and K.-H. Lii, *Inorg. Chem.*, 2002, **41**, 3929.
8 $^1_\infty${[C$_6$N$_2$H$_{14}$][Fe$_2$F$_2$(HPO$_4$)$_2$(H$_2$PO$_4$)$_2$]·2H$_2$O} and $^3_\infty${[C$_6$N$_2$H$_{14}$][Fe$_3$(OH)F$_3$(PO$_4$)(H$_2$PO$_4$)$_2$]$_2$·H$_2$O}: S. Mahesh, M. A. Green and S. Natarajan, *J. Solid State Chem.*, 2002, **165**, 334.
9 $^2_\infty${[4,4′-H$_2$bipy][V$_2$(HPO$_4$)$_4$(4,4′-bipy)$_2$]} (bipy = bipyridine): C.-H. Huang, L.-H. Huang and K.-H. Lii, *Inorg. Chem.*, 2001, **40**, 2625.
10 $^3_\infty${[Ga$_2$(deta)(PO$_4$)$_2$]·2H$_2$O} (deta = diethylenetriamine): C.-H. Lin, S.-L. Wang and K.-H. Lii, *J. Am. Chem. Soc.*, 2001, **123**, 4649.
11 $^3_\infty${[H$_3$O][AlP$_2$O$_6$(OH)$_2$]}: W. Yan, J. Yu, Z. Shi and R. Xu, *J. Chem. Soc., Chem. Commun.*, 2000, 1431.
12 Metal phosphates from amine phosphates: C. N. R. Rao, S. Natarajan and S. Neeraj, *J. Solid State Chem.*, 2000, **152**, 302.
13 $^3_\infty${[H$_3$N(CH$_2$)$_4$NH$_3$]$_2$[Ga$_4$(HPO$_4$)(PO$_4$)$_3$(OH)$_3$]·~5.4H$_2$O}: A. M. Chippindale, K. J. Peacock and A. J. Cowley, *J. Solid State Chem.*, 1999, **145**, 379.
14 $^2_\infty${[Cu(bipy)$_2$(VO)$_3$(PO$_4$)$_2$(HPO$_4$)$_2$]·2H$_2$O} and $^1_\infty$[Cu(terpy)$_2$-(VO$_2$)$_3$(PO$_4$)(HPO$_4$)$_2$]: R. Finn and J. Zubieta, *J. Chem. Soc., Chem. Commun.*, 2000, 1321.
15 J. M. Thomas and R. Raja, *Aust. J. Chem.*, 2001, **54**, 551.
16 S. K. Mohapatra, B. Sahoo, W. Keune and P. Selvam, *J. Chem. Soc., Chem. Commun.*, 2002, 1466.
17 E. Roland and P. Kleinschmit, *Ullmann's Encyclopedia of Industrial Chemistry. Volume A28*, VCH, Weinheim, 5th edn., 1996, p. 475; G. H. Kühl and C. T. Kresge, *Kirk–Othmer Encyclopedia of Chemical Technology. Volume 16*, Wiley, New York, 4th edn., 1995, p. 888; F. Schüth, *Chem. Unserer Zeit*, 1995, **29**, 42; W. Hölderich, M. Hesse and F. Näumann, *Angew. Chem., Int. Ed. Engl.*, 1988, **27**, 226; L. Puppe, *Chem. Unserer Zeit*, 1986, **20**, 117.
18 $^1_\infty$[Cu(H$_2$PO$_4$)$_2$(4,4′-bipy)(H$_2$O)$_2$]: K. Abu-Shandi, C. Janiak and B. Kersting, *Acta Crystallogr., Sect. C*, 2001, **57**, 1261.
19 Reduced molybdenum phosphates: R. C. Haushalter and L. A. Mundi, *Chem. Mater.*, 1992, **4**, 31.
20 $^1_\infty${[(HN(CH$_2$CH$_2$)$_3$NH)K$_{1.35}$][V$_5$O$_9$(PO$_4$)$_2$]·xH$_2$O}: M. I. Khan, L. M. Meyer, R. C. Haushalter, A. L. Schweiter, J. Zubieta and J. L. Dye, *Chem. Mater.*, 1996, **8**, 43.
21 Review: S. Oliver, A. Kuperman and G. A. Ozin, *Angew. Chem., Int. Ed. Engl.*, 1998, **37**, 46.
22 $^1_\infty${[Ga$_4$(C$_{10}$H$_9$N$_2$)$_2$(PO$_4$)(H$_{0.5}$PO$_4$)$_2$(HPO$_4$)$_2$(H$_2$PO$_4$)$_2$(H$_2$O)$_2$]·H$_2$O}: C.-Y. Chen, F. R. Lo, H. M. Kao and K. H. Lii, *J. Chem. Soc., Chem. Commun.*, 2000, 1061.
23 $^1_\infty${[C$_4$N$_2$H$_{12}$]$_2$[Cu$_2$I$_6$]·H$_2$O}: A. B. Corradi, M. R. Cramarossa, T. Manfredini, L. P. Battaglia, G. Pelosi, A. Saccani and F. Sandrolini, *J. Chem. Soc., Dalton Trans.*, 1993, 3587.
24 $^2_\infty${[C$_4$N$_2$H$_{12}$]$_3$[Mo$_8$O$_{27}$]}: W. T. A. Harrison, L. L. Dussack and A. J. Jacobson, *Acta Crystallogr., Sect. C*, 1996, **52**, 1075.
25 $^3_\infty${[C$_4$N$_2$H$_{12}$][(Co$_{0.44}$Zn$_{0.56}$)$_2$(PO$_4$)(H$_{1.5}$PO$_4$)$_2$} and $^3_\infty${[C$_5$N$_2$H$_{14}$]-[(Co$_{0.25}$Zn$_{0.75}$)(HPO$_4$)$_2$]}: A. N. Christensen, A. Bareges, R. B. Nielsen, R. G. Hazell, P. Norby and J. C. Hanson, *J. Chem. Soc., Dalton Trans.*, 2001, 1611.
26 $^1_\infty${[C$_5$N$_2$H$_{13}$][CoCl$_3$(C$_5$N$_2$H$_{12}$)]}: A. Marzotto, D. A. Clemente and G. Valle, *Acta Crystallogr., Sect. C*, 1999, **55**, 43.
27 Hydrothermal synthesis: R. I. Walton, *Chem. Soc. Rev.*, 2002, **31**, 230; A. Stein, S. W. Keller and T. E. Mallouk, *Science (Washington, D. C.)*, 1993, **259**, 1558.
28 F. L. Wagenaar and J. F. Kerwin, *J. Org. Chem.*, 1993, **58**, 4331.
29 E. Craven, K. Abu-Shandi and C. Janiak, *Z. Anorg. Allg. Chem.*, 2003, **629**, 195.
30 Review: P. Gütlich, A. Hauser and H. Spiering, *Angew. Chem., Int. Ed. Engl.*, 1994, **33**, 2024; O. Kahn, *Molecular Magnetism*, VCH, Weinheim, 1993, ch. 4, p. 53ff; J. Zarembowitch, *New J. Chem.*, 1992, **16**, 255; P. Gütlich and A. Hauser, *Coord. Chem. Rev.*, 1990, **97**, 1; H. Toftlund, *Coord. Chem. Rev.*, 1989, **94**, 67; E. König, *Progr. Inorg. Chem.*, 1987, **35**, 527; P. Gütlich, *Struct. Bond.*, 1981, **44**, 83; H. A. Goodwin, *Coord. Chem. Rev.*, 1976, **18**, 293.
31 B. Kersting, M. J. Kolm and C. Janiak, *Z. Anorg. Allg. Chem.*, 1998, **624**, 775; B. Kersting, D. Siebert, D. Volkmer, M. J. Kolm and C. Janiak, *Inorg. Chem.*, 1999, **38**, 3871; A. Geiß, M. J. Kolm, C. Janiak and H. Vahrenkamp, *Inorg. Chem.*, 2000, **39**, 4037.
32 T. Manago, S. Hayami, H. Oshio, S. Osaki, H. Hasuyama, R. H. Herber and Y. Maeda, *J. Chem. Soc., Dalton Trans.*, 1999, 1001.
33 J. R. D. DeBord, W. M. Reiff, C. J. Warren, R. C. Haushalter and J. Zubieta, *Chem. Mater.*, 1997, **9**, 1994.
34 D. Lee, J. L. DuBois, B. Pierce, B. Hedman, K. O. Hodgson, M. P. Hendrich and S. J. Lippard, *Inorg. Chem.*, 2002, **41**, 3172; W. E. Buschmann, J. Ensling, P. Gütlich and J. S. Miller, *Chem. Eur. J.*, 1999, **5**, 3019; J. R. Haradorn, L. Que, Jr and W. B. Tolman, *J. Am. Chem. Soc.*, 1999, **121**, 9760; M. Sato, Y. Hayashi, T. Tsuda and M. Katada, *Inorg. Chim. Acta*, 1997, **261**, 113; C.-C. Wu, H. G. Jang, A. L. Rheingold, P. Gütlich and D. N. Hendrickson, *Inorg. Chem.*, 1996, **35**, 4137.
35 N. N. Greenwood and T. C. Gibb, *Mössbauer Spectroscopy*, Chapman and Hall, London 1971.

36 M. Riou-Cavellec, C. Serre, J. Robino, M. Noguès, J.-M. Grenèche and G. Férey, *J. Solid State Chem.*, 1999, **147**, 122.
37 L.-M. Zheng, H.-H. Song, C.-H. Lin, S.-L. Wang, Z. Hu, Z. Yu and X.-Q. Xin, *Inorg. Chem.*, 1999, **38**, 4618.
38 J. R. D. DeBord, W. M. Reiff, R. C. Haushalter and J. Zubieta, *J. Solid State Chem.*, 1996, **125**, 186.
39 C.-Y. Huang, S.-L. Wang and K.-H. Lii, *J. Porous Mater.*, 1998, **5**, 147.
40 $^{1}_{\infty}\{[C_4N_2H_{12}]_{1.5}[Fe_2(OH)(PO_4)(HPO_4)_2(H_2PO_4)]\cdot 0.5H_2O\}$: V. Zima and K.-H. Lii, *J. Chem.Soc., Dalton Trans.*, 1998, 4109.
41 A. Choudhury, S. Natarajan and C. N. R. Rao, *J. Chem. Soc., Chem. Commun.*, 1999, 1305.
42 V. Zima, K.-H. Lii, N. Nguyen and A. Ducouret, *Chem. Mater.*, 1998, **10**, 1914.
43 M. Cavellec, G. Férey and J. M. Grenèche, *J. Magn. Magn. Mater.*, 1997, **167**, 57.
44 M. Cavellec, D. Riou and G. Férey, *Acta Crystallogr., Sect. C*, 1994, **50**, 1379.
45 Calcuation with PLATON for Windows based on gridpoints at least 1.2 Å away from the nearest van der Waals surface: A. L. Spek, *Acta Crystallogr., Sect. A*, 1990, **46**, C34; PLATON version 29-11-98. *Windows implementation*: L. J. Farrugia, University of Glasgow, Scotland 1997.
46 A. Choudhury and S. Natarajan, *Proc. Indian Acad. Sci. (Chem. Sci.)*, 1999, **111**, 627.
47 *STOE WinXpow*, Version 1.06, copyright 1999, STOE & Cie GMBH. ICSD Inorganic Crystal Structure Database, FIZ Karlsruhe, February 1995.
48 τ = (difference between the two largest anges)/60 for five-coordinated metal centers allows for the assignment of a square-pyramidal (ideally $\tau = 0$) or a trigonal-biypramidal geometry (ideally $\tau = 1$): A. W. Addison, T. N. Rao, J. Reedijk, J. van Rijn and G. C. Verschoor, *J. Chem. Soc., Dalton Trans.*, 1984, 1349.
49 Bond valences (s) calculated from the bond lengths (R) according to $s = \exp(R_0–R)/B$ and $R_0 = 1.759$ for Fe^{3+}–O, $B = 0.37$; *Program VALENCE* (Version 2.00, February 1993); I. D. Brown, *J. Appl. Crystallogr.*, 1996, **29**, 479.
50 I. D. Brown and R. D. Shannon, *Acta Crystallogr., Sect. A*, 1973, **29**, 266; I. D. Brown and K. K. Wu, *Acta Crystallogr., Sect. B*, 1976, **32**, 1957; I. D. Brown and D. Altermatt, *Acta Crystallogr., Sect. B*, 1985, **41**, 244.
51 V. Zima and K.-H. Lii, *J. Solid State Chem.*, 1998, **139**, 326.
52 L.-M. Zheng, X. Fang, K.-H. Lii, H.-H. Song, X.-Q. Xin, H.-K. Fun, K. Chinnakali and I. A. Razak, *J. Chem. Soc., Dalton Trans.*, 1999, 2311; N. Okabe and T. Makino, *Acta Crystallogr., Sect. C*, 1998, **54**, 1279; P. Laine, A. Gourdon and J.-P. Launay, *Inorg. Chem.*, 1995, **34**, 5129; P. Laine, A. Gourdon and J.-P. Launay, *Inorg. Chem.*, 1995, **34**, 5138.
53 J. Sletten, H. Daraghmeh, F. Lloret and M. Julve, *Inorg. Chim. Acta*, 1998, **127**, 279; E. Andres, G. De Munno, M. Julve, J. A. Real and F. Lloret, *J. Chem. Soc., Dalton Trans.*, 1993, 2169.
54 Q. Liu, Y. Wei, W. Wang and S. Zhang, *Acta Crystallogr., Sect. C*, 1999, **55**, 9900127; S. Noro, M. Kondo, S. Kitagawa, T. Ishii and H. Matsuzaka, *Chem. Lett*, 1999, 727; J. M. C. Juan, C. Mackiewicz, M. Verelst, F. Dahan, A. Bousseksou, Y. Sanakis and J.-P. Tuchagues, *Inorg. Chem.*, 2002, **41**, 1478.
55 M. Tiliakos, P. Cordopatis, A. Terzis, C. P. Raptopoulou, S. P. Perlepes and E. M. Zoupa, *Polyhedron*, 2001, **20**, 2203; S. Kiani, A. Tapper, R. J. Staples and P. Stavropoulos, *J. Am. Chem. Soc.*, 2000, **122**, 7503.
56 A. Neves, M. A. de Brito, I. Vencato, V. Drago, K. Griesar, W. Haase and Y. P. Mascarenhas, *Inorg. Chim. Acta*, 1993, **5**, 214; A. Neves, M. A. de Brito, I. Vencato, V. Drago, K. Griesar and W. Haase, *Inorg. Chem.*, 1996, **35**, 2360; D. Zirong, S. Bhattacharya, J. K. McCusker, P. M. Hagen, D. N. Hendrickson and C. G. Pierpont, *Inorg. Chem.*, 1992, **31**, 870.
57 Y. Feng, S.−L. Ong, J. Hu and W. J. Ng, *Acta Crystallogr., Sect. C*, 2002, **58**, m34; A. Horn, A. Neves, A. J. Bortoluzzi, V. Drago and W. A. Ortiz, *Inorg. Chem. Commun.*, 2001, **4**, 173; E. J. Seddon, J. Yoo, K. Folting, J. C. Huffman, D. N. Hendrickson and G. Christou, *J. Chem. Soc., Dalton Trans.*, 2000, 3640; C. M. Grant, M. J. Knapp, J. C. Huffman, D. N. Hendrickson and G. Christou, *J. Chem. Soc., Chem. Commun.*, 1998, 1753; C. M. Grant, M. J. Knapp, W. E. Streib, J. C. Huffman, D. N. Hendrickson and G. Christou, *Inorg. Chem.*, 1998, **37**, 6065; S. M. Gorun and S. J. Lippard, *Inorg. Chem.*, 1988, **27**, 149; A. J. Blake, C. M. Grant, S. Parsons, G. A. Solan and R. E. P. Winpenny, *J. Chem. Soc., Dalton Trans.*, 1996, 321.
58 R. W. Saalfrank, I. Bernt, M. M. Chowdhry, F. Hampel and G. B. M. Vaughan, *Chem. Eur. J.*, 2001, **7**, 2765; E. J. Seddon, J. C. Huffman and G. Christou, *J. Chem. Soc., Dalton Trans.*, 2000, 4446; P. J. Zapf, R. P. Hammond, R. C. Haushalter and J. Zubieta, *Chem. Mater.*, 1998, **10**, 1366.
59 A. K. Boudalis, N. Lalioti, G. A. Spyroulias, C. P. Raptopoulou, A. Terzis, V. Tangoulis and S. P. Perlepes, *J. Chem. Soc., Dalton Trans.*, 2001, 955; K. A. Abboud, C. Xu and R. S. Drago, *Acta Crystallogr., Sect. C*, 1998, **54**, 1270; K. L. Taft, A. Masschelein, S. Liu, S. J. Lippard, D. G-Shweky and A. Bino, *Inorg. Chim. Acta*, 1992, **198**, 627.
60 K. Abu-Shandi, H. Winkler, M. Gerdan, F. Emmerling, B. Wu and C. Janiak, *Dalton Trans.*, 2003, DOI: 10.1039/b301610b.
61 C. E. Buss and K. R. Mann, *J. Am. Chem. Soc.*, 2002, **124**, 1031; E. J. Cussen, J. B. Claridge, M. J. Rosseinsky and C. J. Kepert, *J. Am. Chem. Soc.*, 2002, **124**, 9574.
62 M. Hartmann and S. Ernst, *Angew. Chem., Int. Ed.*, 2000, **39**, 888; P. A. MacFaul, D. D. M. Wayner and K. U. Ingold, *Acc. Chem. Res.*, 1998, **31**, 159.
63 *Activation and Functionalization of Alkanes*, ed. C. L. Hill, Wiley: Chichester, 1989; ch. 6–8; P. A. MacFaul, K. U. Ingold, D. D. M. Wayner and L. Que, Jr., *J. Am. Chem. Soc.*, 1997, **119**, 10594; P. A. MacFaul, I. W. C. E. Arends, K. U. Ingold and D. D. M. Wayner, *J. Chem. Soc., Perkin Trans. 2*, 1997, 135.
64 R. Raja, G. Sankar and J. M. Thomas, *J. Am. Chem. Soc.*, 1999, **121**, 11926.
65 J. M. Thomas, R. Raja, G. Sankar and R. G. Bell, *Acc. Chem. Res.*, 2001, **34**, 191.
66 J. M. Thomas, R. Raja, G. Sankar and R. G. Bell, *Nature (London)*, 1999, **398**, 227; R. Raja, G. Sankar and J. M. Thomas, *J. Chem. Soc., Chem. Commun.*, 1999, 829.
67 K. Abu-Shandi and C. Janiak, unpublished work.
68 *SMART*, Data Collection Program for the CCD Area-Detector System; *SAINT*, Data Reduction and Frame Integration Program for the CCD Area-Detector System, Bruker Analytical X-ray Systems, Madison, Wisconsin, USA, 1997.
69 G. Sheldrick, Program *SADABS*: Area-detector absorption correction, University of Göttingen, Germany, 1996.
70 G. M. Sheldrick, *SHELXS-97, SHELXL-97*, Programs for Crystal Structure Analysis, University of Göttingen, Germany, 1997.
71 DIAMOND 2.1e for Windows. Crystal Impact Gbr, Bonn, Germany.; http://www.crystalimpact.com/diamond.